JCB: **Article**

Myosin concentration underlies cell size–dependent scalability of actomyosin ring constriction

Meredith E.K. Calvert,[1,2] Graham D. Wright,[3] Fong Yew Leong,[4] Keng-Hwee Chiam,[4,5] Yinxiao Chen,[1] Gregory Jedd,[1,6] and Mohan K. Balasubramanian,[1,2,5,6]

[1]Temasek Life Sciences Laboratory, The National University of Singapore, Singapore 117604
[2]Marine Biological Laboratory, Woods Hole, MA 02543
[3]Institute of Medical Biology, A*STAR, Immunos, Singapore 138648
[4]Institute of High Performance Computing, A*STAR, Singapore 138632
[5]Mechanobiology Institute and [6]Department of Biological Sciences, The National University of Singapore, Singapore 117543

In eukaryotes, cytokinesis is accomplished by an actomyosin-based contractile ring. Although in *Caenorhabditis elegans* embryos larger cells divide at a faster rate than smaller cells, it remains unknown whether a similar mode of scalability operates in other cells. We investigated cytokinesis in the filamentous fungus *Neurospora crassa*, which exhibits a wide range of hyphal circumferences. We found that *N. crassa* cells divide using an actomyosin ring and larger rings constricted faster than smaller rings. However, unlike in *C. elegans*, the total amount of myosin remained constant throughout constriction, and there was a size-dependent increase in the starting concentration of myosin in the ring. We predict that the increased number of ring-associated myosin motors in larger rings leads to the increased constriction rate. Accordingly, reduction or inhibition of ring-associated myosin slows down the rate of constriction. Because the mechanical characteristics of contractile rings are conserved, we predict that these findings will be relevant to actomyosin ring constriction in other cell types.

Introduction

Throughout biology there are examples of cellular mechanisms regulated by cell size. Size dependence governs cell cycle signaling, as in the initiation of mitosis in the fission yeast *Schizosaccharomyces pombe* (Nurse, 1975) and also structural processes of cell division, such as the length and rate of spindle elongation in *Caenorhabditis elegans* (Hara and Kimura, 2009). The rate of cytokinesis was recently determined to depend on cell size in *C. elegans* embryos (Carvalho et al., 2009). In these cells, the duration of ring closure was constant and independent of starting size, implying that the contractile rings of larger cells must constrict at a faster rate than those of smaller cells. This size-dependent variation in the rate of constriction was scalable, such that a cell with twice the perimeter constricted at twice the rate. This resulted in the total duration of cytokinesis remaining uniform between subsequent embryonic divisions (Carvalho et al., 2009).

In the majority of eukaryotes cytokinesis is accomplished by the constriction of a cortical actomyosin-based ring (Balasubramanian et al., 2004; Barr and Gruneberg, 2007; Stark et al., 2010). It is established that F-actin and a number of actin-binding proteins form the structural framework of the ring (Maupin and Pollard, 1986; Pelham and Chang, 2002; Field et al., 2005). Myosin II motors associate with the actin filaments at the ring and are thought to provide the predominant contractile force by regulating actin turnover and disassembly (Mabuchi and Okuno, 1977; Guha et al., 2005; Murthy and Wadsworth, 2005). Though well conserved, the precise architecture of these interactions and the mechanism by which myosin II promotes actin turnover and contractility during cytokinesis has yet to be fully elucidated.

To determine if scalability of the rate of cytokinesis is also a property of contractile actomyosin rings in fungi, we investigated septum formation in the filamentous fungus, *N. crassa*. In this organism a wide range of hyphal diameters are observed within a single colony, and septum formation is preceded by the assembly and constriction of an actin ring (Rasmussen and Glass, 2005). We performed live-cell imaging of F-actin and myosin II during septation and found that both the rate and the total

M.E.K. Calvert and G.D. Wright contributed equally to this paper.
Correspondence to Meredith E.K. Calvert: meredith@tll.org.sg

The Rockefeller University Press $30.00
J. Cell Biol. Vol. 195 No. 5   799–813
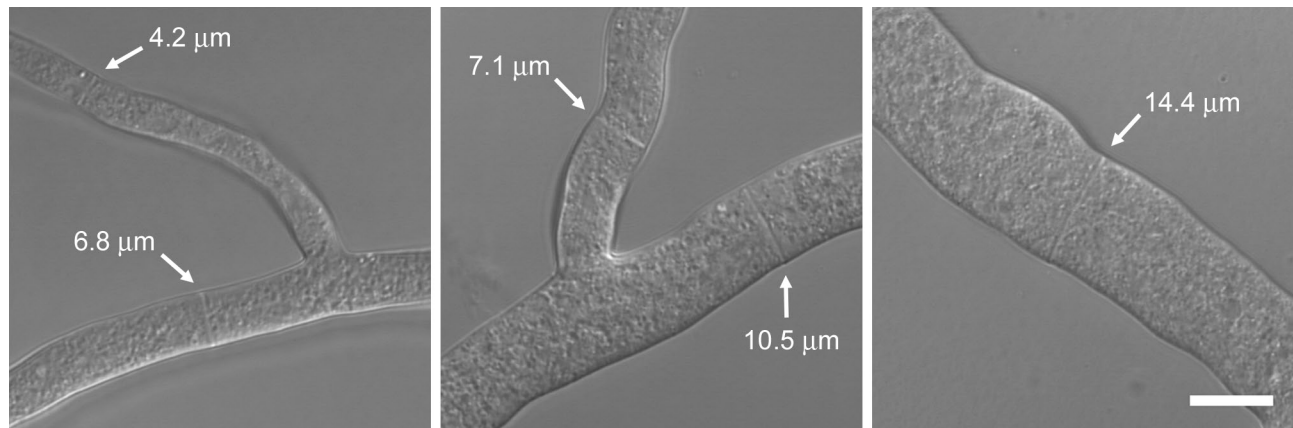www.jcb.org/cgi/doi/10.1083/jcb.201101055

JCB   799

Figure 1. **Range of hyphal diameters observed in *N. crassa*.** White arrows indicate positions and diameters of septa. All images are to the same scale. Bar, 10 µm.

duration of cytokinesis increased with increasing cell size. We examined the dynamics of the ring components both during ring assembly and throughout constriction and determined that the amount of myosin incorporated into the assembling ring also increases with ring size. Here, we demonstrate that the rate of ring constriction is mediated by both the amount and the activity of ring-associated myosin, and that myosin is therefore a likely determinant of the size-dependent scalability of ring constriction.

Results

N. crassa is an attractive model for studies of scalability

To investigate the potentially size-dependent scalability of the rate of cytokinesis within nonembryonic cells, we sought a model system in which cellular diameter varied significantly among wild-type cells. Primary and secondary hyphae in *N. crassa* exhibit large differences in diameter, and within a single colony we observed up to a fourfold range in hyphal diameter (Fig. 1). Given this intrinsic variation in size, its genetic tractability, and the ease of live-cell confocal imaging, we concluded that *N. crassa* is an attractive model for studying the scalability of the rate of cytokinesis.

Identification of conserved actomyosin ring components in *N. crassa*

In *N. crassa*, septation occurs at frequent intervals along the length of the hyphae, and actin has been shown to localize to the sites of septation (Rasmussen and Glass, 2005; Berepiki et al., 2010). In another filamentous fungus, *Aspergillus nidulans*, homologues of a number of well-known regulators of cytokinesis have been characterized, including α-actinin (Bruno et al., 2001; Wang et al., 2009) and the formin, SepA (Harris et al., 1997). Though actin rings are known to be involved in septation in *N. crassa*, other components of the contractile ring have not been well characterized in this organism. To determine whether proteins important for actomyosin ring function and cytokinesis in higher eukaryotes are conserved in *N. crassa*, a BLAST search was performed within the genome (Galagan et al., 2003) to identify conserved actomyosin ring

components. Homologues of the majority of ring components were found to be present. Thus, the structural features of the contractile actomyosin ring are likely to be well conserved within this organism (Table I).

Septation in *N. crassa* is regulated by type II myosin

Type II myosin motors drive actomyosin ring constriction during cytokinesis in most eukaryotic organisms (Mabuchi and Okuno, 1977; Maupin and Pollard, 1986; De Lozanne and Spudich, 1987; Knecht and Loomis, 1988; Manstein et al., 1989; May et al., 1997; Shelton et al., 1999). By in silico genomic analysis we determined that only one type II myosin gene is encoded in the genome of *N. crassa*, referred to hereafter as *myo2*. Upon further characterization, the *N.crassa myo2* gene was found to span approximately 7.3 kb, and be comprised of three coding exons interrupted by two short introns and followed by a 301 bp 3′ UTR (Fig. 2 A). Determination of the complete coding sequence of *myo2* revealed that it encodes a protein of 2,418 amino acids consisting of an N-terminal SH3 domain and myosin head (motor domain) and a C-terminal myosin tail (Fig. 2 A). Sequence comparison showed the region of highest homology among eukaryotes is within the motor domain (56% identity and 39% identity with myosin heavy chain from *S. pombe* and *H. sapiens*, respectively). To determine the gene function, we examined septation in a *myo2*-deleted strain. In wild-type cells septa were observed within all hyphae with an approximate frequency of two septa within 50 µm from branch sites (see arrows in Fig.1 and Fig. 2 B). By contrast, a sublethal *myo2*-deleted heterokaryon strain was completely lacking in observable septa (Fig. 2 C), suggesting that septation is defective when myosin II function is compromised. To observe the localization and dynamics of myosin II within the division apparatus during septation in *N. crassa*, we constructed a strain expressing myosin II as a GFP fusion protein under control of its native promoter at its genomic location. Myo2-GFP appeared as a diffuse cortical band of 1–2 µm before septation (Fig. 2 D; 0 min) and then compacted into a dense ring structure at the onset of ring constriction. As constriction proceeded, Myo2-GFP remained tightly associated with the contractile apparatus until the completion

Table I. **Conservation of actomyosin ring components among divergent eukaryotes**

Protein	S. pombe	C. elegans	N. crassa
Profilin	Cdc3 (Balasubramanian et al., 1994)	Pfn-1 (Severson et al., 2002)	S.p, C.e. NCU06397*
Myosin essential light chain	Cdc4 (McCollum et al., 1995)	ND	S.p. CU06617*
Tropomyosin	Cdc8 (Balasubramanian et al., 1992)	Tmy-1 (Ono and Ono, 2004)	S.p. NCU01204*, C.e. NCU01878
F-BAR domain–containing protein	Cdc15 (Fankhauser et al., 1995)	ND	S.p. NCU10905
Formin	Cdc12 (Chang et al., 1997)	Cyk-1 (Severson et al., 2002)	S.p., C.e. NCU01431* (SepA)
Myosin type II heavy chain	Myo2 (Kitayama et al., 1997; May et al., 1997)	Nmy-2 (Shelton et al., 1999)	S.p., C.e. NCU00551
Actin	Act1 (Ishiguro and Kobayashi, 1996)	Act-1/3, Act-2, Act-3 (Velarde et al., 2007)	S.p., C.e. NCU04173*, NCU04247*
ADF/cofilin	Adf1 (Nakano and Mabuchi, 2006)	Unc-60 (McKim et al., 1994)	S.p., C.e. NCU01587
IQGAP	Rng2 (Eng et al., 1998)	Pes-7 (Skop et al., 2004)	S.p., C.e. NCU03116* (ras-GAP)
UCS domain–containing protein	Rng3 (Balasubramanian et al., 1998)	Unc-45 (Kachur et al., 2004)	S.p., C.e. NCU06821* (Cro1)
Myosin regulatory light chain	Rlc1 (Le Goff et al., 2000; Naqvi et al., 2000)	Mlc-4 (Shelton et al., 1999)	S.p., C.e. NCU04120* (Calmodulin)
Septin	Spn1, Spn2, Spn3, Spn4 (Wu et al., 2003; An et al., 2004)	Unc-59 (Nguyen et al., 2000)	S.p., C.e. NCU08297* (Cdc3), NCU03515* (Cdc10), NCU02464* (septin-1), NCU03795* (Cdc12)
F-BAR domain–containing protein	Imp2 (Demeter and Sazer, 1998)	ND	S.p. NCU10905
Alpha actinin	Ain1 (Wu et al., 2001)	Atn-1 (Barstead et al., 1991)	S.p., C.e. NCU06429
Paxilin	Pxl1 (Ge and Balasubramanian, 2008; Pinar et al., 2008)	ND	S.p. NCU09812.3

Genes encoding proteins homologous to highly conserved actomyosin ring components in both *S. pombe* and *C. elegans* are represented within the *N. crassa* genome. *S. pombe* has been included here because many of the proteins involved in cytokinesis are best characterized in this model system. Asterisk indicates annotated genes. If the name given in the annotation differs from the name of the homologous protein, the given name is indicated in parentheses. ND indicates a homologous role in cytokinesis has not been characterized for this protein. S.p., *S. pombe* homologue; C.e., *C. elegans* homologue.

of septation (Fig. 2 D and Video 1). Observation of labeled membrane using the vital dye FM4-64 (Hickey et al., 2005) and the localization of Myo2-GFP revealed that the ring of myosin II stays at the leading edge of nascent membrane formation throughout constriction (Fig. 2 E).

F-actin assembles into a constricting ring at the septation site in *N. crassa*

We then observed the dynamics of F-actin during septation in *N. crassa* using genomically integrated Lifeact-GFP, a probe shown to bind to actin cables and contractile rings in *N. crassa*, budding yeast, and mammalian fibroblasts (Riedl et al., 2008; Berepiki et al., 2010). Before the initiation of ring constriction, Lifeact-GFP accumulated along a 9–28-μm region of the cortex (Fig. 3 A; 1 min) and then rapidly assembled into a tight ring. After ring assembly, the ring constricted steadily until septation was complete. Lifeact-GFP remained associated with the ring throughout constriction (Fig. 3 A and Video 2). The behavior of both F-actin and myosin II during septation and the lack of septation in cells defective in myosin II establish that *N. crassa* cytokinesis relies upon the function of an actomyosin-based contractile ring.

Ring constriction is followed by invagination of the plasma membrane and cell wall deposition and occurs at a constant rate

Using cell wall and membrane labels (calcofluor and FM4-64, respectively) in conjunction with the Lifeact-GFP actin marker, we observed that ring constriction was tightly coupled with plasma membrane invagination and nascent cell wall deposition at the cleavage site (Fig. 3 B and Video 3). As was observed with myosin II, actin occupied the leading edge of the contractile ring, and new membrane deposition followed centripetally behind the closing ring. Analysis of kymographs and graphical plots of the of ring constriction over time in individual cells revealed that, once initiated, the constriction occurred at a constant rate (Figs. 2 E, 3 C, and 4 A).

The rate of ring constriction in *N. crassa* increases with increasing cell size

In early *C. elegans* embryos, the scalability of the rate of ring constriction causes the duration of cytokinesis to be constant and independent of the starting cell size (Carvalho et al., 2009). Given that the hyphae in *N. crassa* are cylindrical in shape with a circular cross-section perpendicular to the plane of growth (as seen in Fig. 3 B), we calculated ring circumference as $2\pi r_c$ where r_c is the ring radius, and determined that the starting circumference of the contractile ring varied between 12 and 48 μm in our sample population. We measured the decrease in actomyosin ring circumference during constriction over time from hyphae with a range of circumferences (Fig. 4 A). Interestingly, the rate of ring constriction was higher in hyphae with a larger circumference. Smaller hyphae (circumference of ∼15 μm) constricted at 0.07 μm/s on average, whereas larger hyphae with threefold the circumference (∼45 μm) constricted at less than threefold the rate of smaller hyphae, at an average rate of 0.17 μm/s (Fig. 4 B). We therefore refer to this increased rate
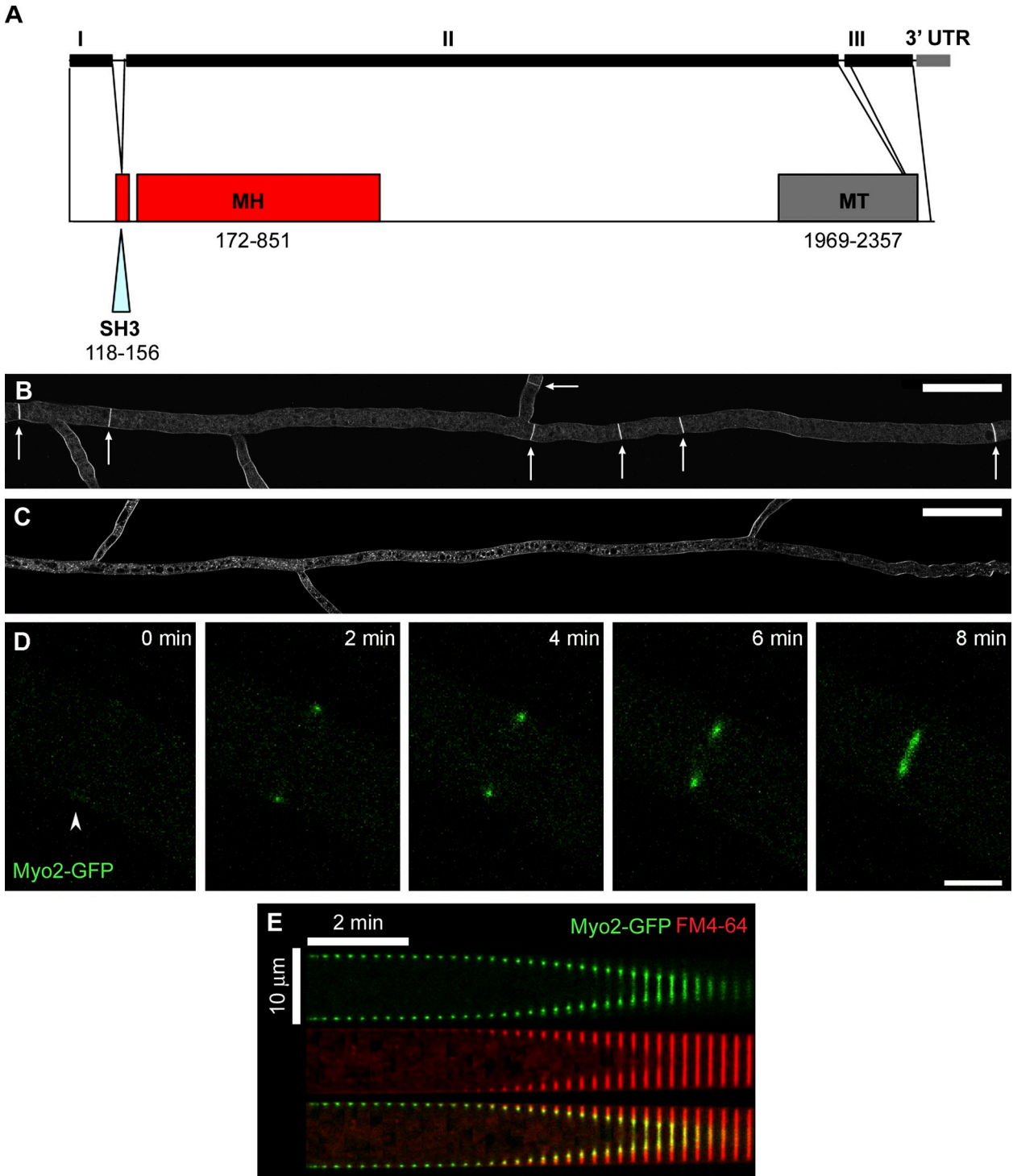
Figure 2. **Characterization of Myosin II in *N. crassa*.** (A) Schematic representation of *N. crassa myo2* gene structure and the corresponding encoded protein domains (drawn to scale). The three coding exons (I, II, and III), two small introns, and 3' UTR are indicated. SH3, SH3 domain; MH, myosin head (motor domain); MT, myosin tail. Numbering indicates the corresponding amino acid residues within the protein sequence. (B) Septa in a wild-type *N. crassa* strain. The wild-type FGSC#9719 strain was labeled with FM4-64 to visualize membranes and septa. White arrows indicate positions of septa. The image was created from 11 overlapping individual confocal images by merging and cropping in Adobe Photoshop. Bar, 50 µm. (C) Septation is defective in a heterokaryon knockout strain of the myosin II homologue, NCU00551. NCU00551 deleted heterokaryons were labeled with FM4-64 to visualize membranes and septa. The image was created from 12 overlapping individual confocal images by merging and cropping in Adobe Photoshop. Bar, 50 µm. (D) Myo2-GFP localized to a discreet region on the hyphal cortex, assembled into a contractile ring, and persisted at the ring throughout septation. The time is indicated in minutes; arrowhead indicates the region of preassembly accumulation. Bar, 5 µm. See also Video 1. (E) A kymograph showing the decrease in ring diameter over time within a representative hypha expressing Myo2-GFP (green) and membranes labeled with FM4-64 (red) and a merge of the two.
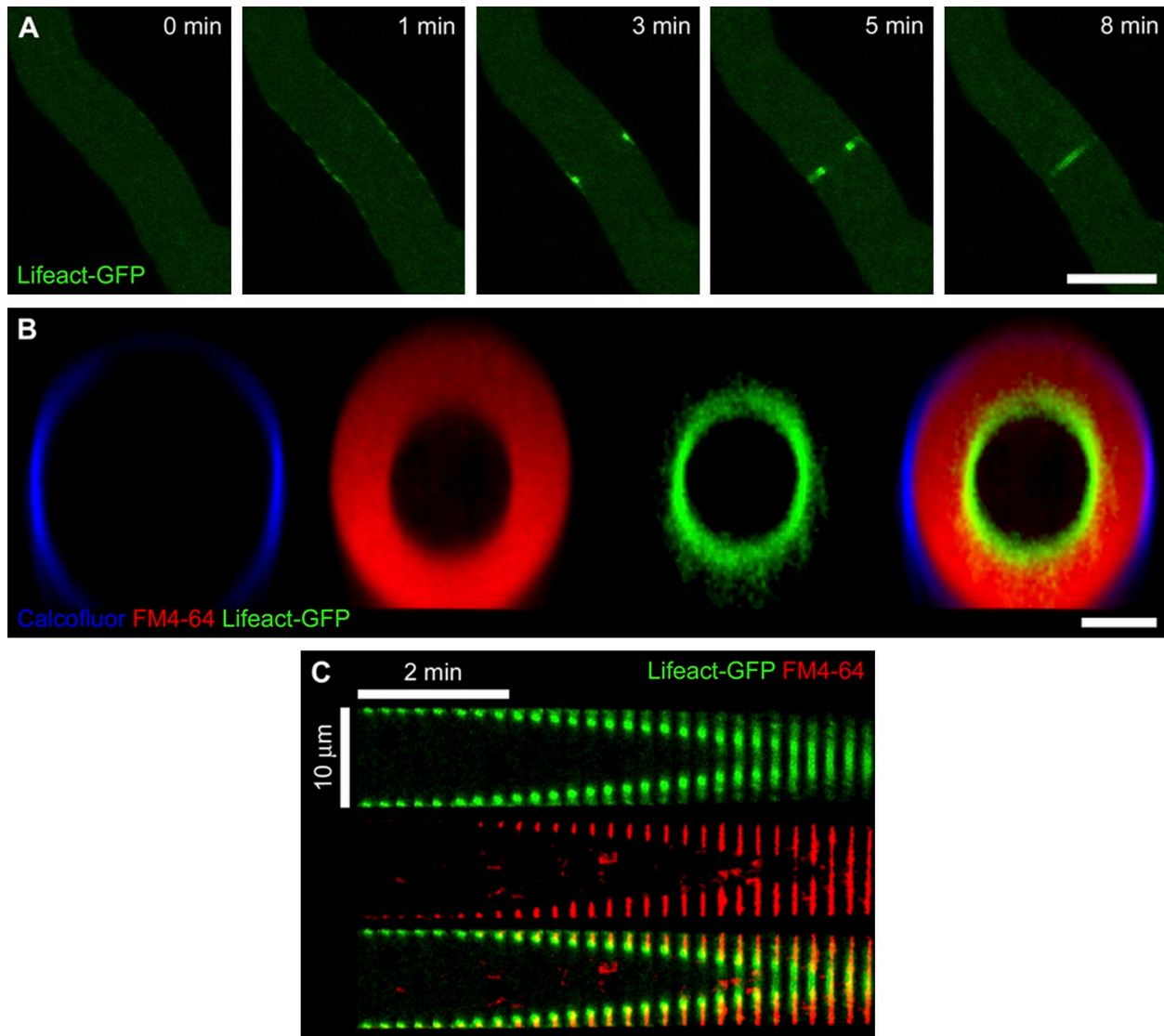
Figure 3. **F-actin localization at the division site in** *N. crassa.* (A) The actin-binding probe Lifeact-GFP accumulated along the hyphal cortex, assembled into a contractile ring, and persisted at the ring throughout septation. The time is indicated in minutes. Bar, 10 μm. See also Video 2. (B) Actomyosin ring constriction was observed using Lifeact-GFP (green), FM4-64 (red), and calcofluor (blue) to label actin, cell membrane, and cell wall, respectively. Image shows a transverse section of a representative cell during ring constriction. Bar, 5 μm. See also Video 3. (C) A kymograph showing the decrease in ring diameter over time within a representative hypha expressing Lifeact-GFP (green) and membranes labeled with FM4-64 (red) and a merge of the two.

of ring constriction in larger hyphae as "partial scalability." The duration of septation, though not constant across hyphae of different sizes, did not show as much of a size-dependent increase as would be predicted if the constriction rate was constant among all cells (Fig. 4 C). During the vegetative growth phase, colonies of *N. crassa* consist of wider, primary hyphae that branch subapically into the narrower secondary hyphae. To rule out the possibility that the detected differences in rate are not size-dependent but in fact due to biological differences between primary and secondary hyphae, we compared the constriction rates of a subset of equally sized primary and secondary hyphae. There was no difference in the mean rate of constriction due to hyphal rank alone (Fig. S1). Together, these experiments led to the conclusion that, as in *C. elegans* embryonic cells, the rate of actomyosin ring constriction in *N. crassa* increases substantially with increasing cell size.

Larger rings initiate constriction with a higher concentration of myosin II

In order for myosin or actin to be providing scalability to our system, we expected to see an increased total amount of the potential rate-determinant protein with increasing hyphal circumference. We measured the fluorescence intensity of Myo2-GFP and Lifeact-GFP at the initiation of constriction and quantified the total amount of both markers present in the ring. The total amount of both of Myo2-GFP and Lifeact-GFP assembled into the ring at the start of ring constriction is higher in larger hyphae (Fig. 5 A). To explore this further, we then measured the amount of each marker per unit length and found that the concentration of Myo2-GFP also increased significantly in larger hyphae whereas the concentration of Lifeact-GFP remained constant and independent of starting circumference (Fig. 5 B). We hypothesize that the increased concentration of myosin II motors
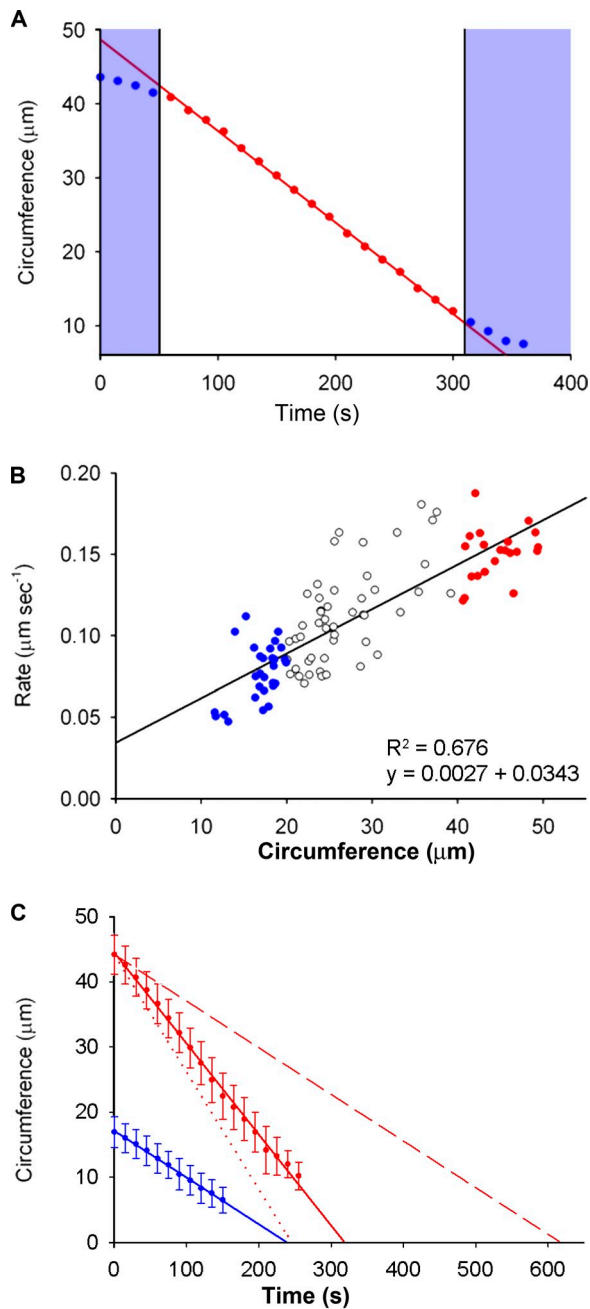
Figure 4. **Rate and duration of actomyosin ring constriction in *N. crassa*.** (A) A graph showing the linear decrease in ring circumference calculated from image analysis of the Lifeact-GFP signal over time in a representative cell. The time points in red correspond to the constant phase of ring constriction; time points in blue show those during ring assembly and at the end of constriction, after the final pore size has been reached. The areas shaded blue were excluded for the calculation of constriction rate. (B) The rate of ring constriction is size dependent and larger rings constrict at a faster rate. Each data point represents the rate measured during the linear phase of constriction for individual rings of initial circumference 10–20 μm (blue), 20–40 μm (white), and > 40 μm (red); n = 98. R^2 values and equations of the lines are indicated. (C) Average duration of constriction in cells with large (mean circumference = 45 μm; red, n = 21) and small (mean circumference = 15 μm; blue, n = 29) initial ring circumference. Each data point represents the mean ring circumference of cells within that size category at a given time during ring constriction. Error bars represent the standard deviation from the mean; n ≥ 10 measurements for each time point. The dotted line indicates the result predicted in large cells if the constriction rate were fully scalable with size, whereas the dashed line indicates that if constriction rate is completely nonscalable and size independent.

in larger hyphae could provide additional contractile force, enabling larger rings to complete constriction at a faster rate than smaller rings.

The concentration of ring-associated myosin II increases during constriction

We then performed further quantitative live-cell confocal microscopy in order to understand the molecular behavior of the ring components during ring constriction. We observed that the intensity of Myo2-GFP within the ring appeared to increase during constriction, whereas the intensity of Lifeact-GFP remained constant. To verify this, we quantified the concentration of Myo2-GFP and Lifeact-GFP associated with the ring by measuring the intensity of both markers during the constant phase of ring constriction. In the 3 min immediately after the initiation of constriction, before completion of septation, the concentration of Myo2-GFP increased by more than 80%, whereas the concentration of Lifeact-GFP remained unchanged (Fig. 6 A). To determine if the amount of myosin II in a given ring is proportional to the ring circumference, we then compared the amount of myosin II within an initially large ring after 3 min of constriction, and that of a smaller ring that initiated constriction at the same size. Larger rings consistently contained more myosin II at 3 min into constriction than smaller rings of the equivalent size, and in all rings we observed that the total amount of myosin II assembled into a ring at the start is retained throughout constriction (Fig. 6, B and C). Examination of the redistribution of myosin during constriction also confirmed that the concentration of myosin II increased during constriction and was always greater in larger rings (Fig. 6 C). Taken together, these data demonstrated first that the total number and concentration of myosin motors associated with the ring is dependent upon the starting hyphal size, and second that the number of myosin motors incorporated into the ring at assembly remains constant throughout ring constriction.

Myosin undergoes turnover during ring constriction

Though previous studies in fission yeast and *Dictyostelium discoideum* have shown that ring-associated myosin II turns over continuously (Yumura, 2001; Pelham and Chang, 2002), more recent work in *C. elegans* and *Drosophila melanogaster* cells found myosin becomes stably associated with the ring after the initiation of constriction (Carvalho et al., 2009; Uehara et al., 2010). To determine whether the individual myosin subunits are stably associated with the ring in *N. crassa*, we performed fluorescence recovery after photobleaching (FRAP) experiments on the Myo2-GFP strain. We photobleached entire rings after the initiation of constriction, and monitored the recovery of the signal across the entire ring in three dimensions (Fig. 7 A and Video 4). Within 2 min after bleaching, Myo2-GFP was again detectable in the constricting ring, and the levels continued to recover until reaching 80% of prebleach levels by the time ring constriction was complete, with a half-time of recovery of 56 s (Fig. 7 B). These data suggest that a significant portion of the individual ring-associated
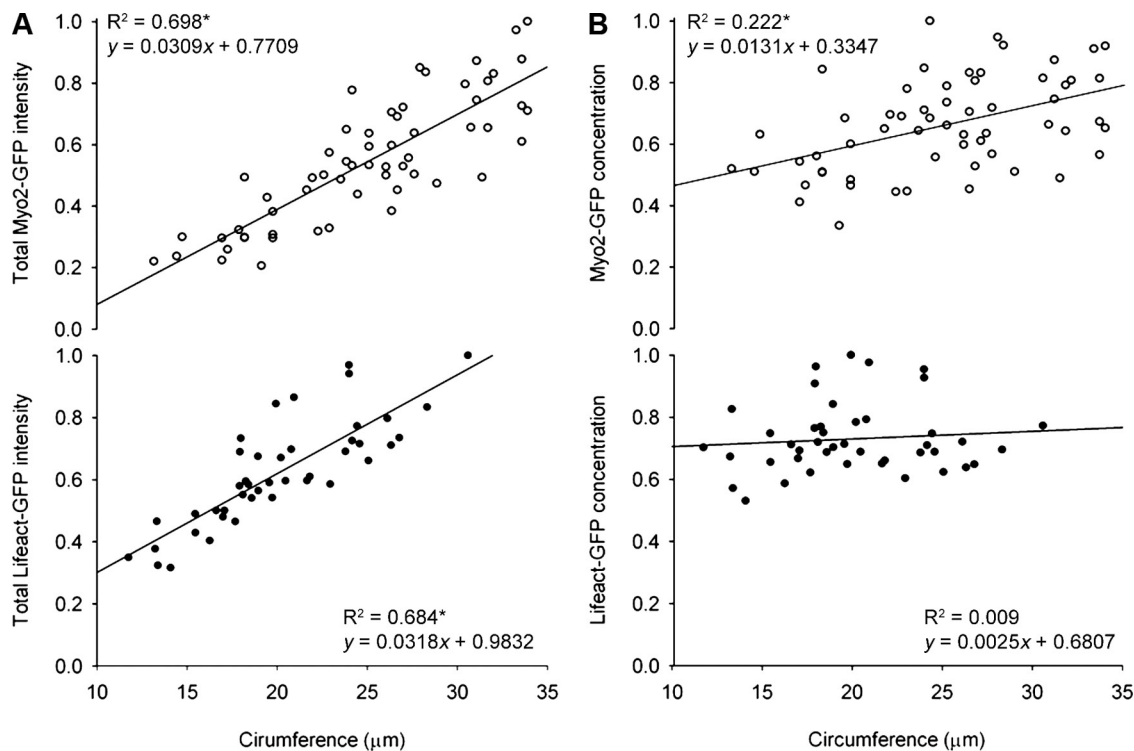
Figure 5. **Quantitation of total amount and concentration of ring-associated F-actin and myosin II.** (A) Total amount of Myo2-GFP (open circles; top, *n* = 59) and Lifeact-GFP (closed circles; bottom, *n* = 43) expressed in relative units of fluorescence intensity, as a function of hyphal circumference at start of constriction. R^2 values and equations of the lines are indicated. Asterisk indicates a correlation coefficient where $P < 0.001$. (B) Concentration of Myo2-GFP (open circles; top, *n* = 59) and Lifeact-GFP (closed circles; bottom, *n* = 43) expressed in relative units of fluorescence intensity per confocal volume, as a function of hyphal circumference at start of constriction. R^2 values and equations of the lines are indicated. Asterisk indicates a correlation coefficient where $P < 0.001$.

myosin II subunits turn over throughout ring constriction, though the total amount remains constant.

Ring constriction requires continual assembly and turnover of actin filaments

In *C. elegans* embryos, ring-associated actin filaments were determined to be stably associated with the contractile ring. Inhibition of new actin polymerization with the drug latrunculin A had no effect on the ability of the ring to constrict, suggesting that constriction is coupled with disassembly, but not turnover, of actin filaments (Carvalho et al., 2009). Though in *N. crassa* the actin appears to be lost progressively from the ring during constriction, whether the actin filaments are stably associated with the ring is not clear from our quantitative fluorescence microscopy alone. Because the recovery dynamics of Lifeact-GFP after FRAP may not accurately reflect that of molecular actin itself, we decided to also use latrunculin A treatment to examine if actin turnover was required for ring constriction. The drug was solubilized in DMSO containing FM4-64 membrane stain in order to monitor uptake. Although the control cells, treated with DMSO only, were able to assemble rings and complete ring constriction normally, latrunculin A caused immediate delocalization of Lifeact-GFP from the ring and stalled septation, as is evident from the incomplete membrane ingression (Fig. 7 C). No ring assembly, ring-associated actin, or ring constriction was observed after latrunculin A treatment. This suggests that continual turnover of actin filaments is required for septation in *N. crassa*.

Decreased ring-associated myosin II activity causes a decreased rate of ring constriction

If the size-dependent increase in the concentration of myosin licenses larger rings to constrict at an increased rate, a simple prediction is that decreasing the amount of ring-associated myosin or myosin activity should slow ring constriction. To test this, we treated live cells with a variety of concentrations of the drug blebbistatin, which has been shown to inhibit myosin II activity by blocking myosin II heads in an actin-detached state (Straight, et al., 2003; Kovács et al., 2004). At a high concentration (1 mM), blebbistatin caused total dissociation of Myo2-GFP from contractile rings and stalled septation completely (Fig. 8 A). At lower concentrations (100 µM), treatment with blebbistatin caused a 15% decrease in the amount of Myo2-GFP at the ring (Fig. 8 B), resulting in constriction rates around half that of control cells of the same size (Fig. 8 C and Video 5). The amount of actin associated with the ring remained unchanged after blebbistatin treatment (Fig. S2). A second approach to perturbing myosin II activity is to genetically alter the protein itself. We observed that the introduction of the C-terminal GFP tag to the endogenous myosin II caused a slight reduction in ring constriction rate relative to the Lifeact-GFP strain (Fig. 8 D), though growth rate, septal frequency, and hyphal morphology were unaffected. To explore this hypomorphic phenotype, we developed a heterokaryon strain in which the amount of Myo2-GFP was reduced to around one third of the
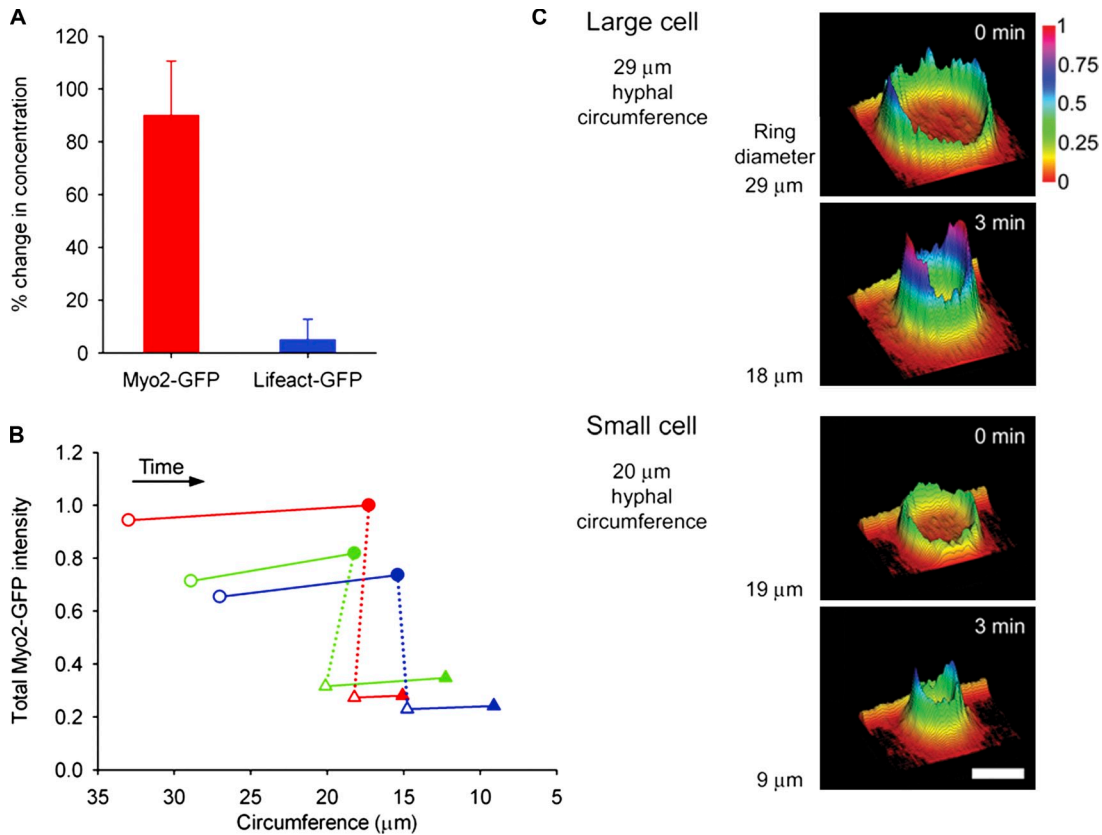
Figure 6. **Concentration of ring-associated F-actin and myosin II during ring constriction.** (A) Change in concentration of Myo2-GFP (red) and Lifeact-GFP (blue) during 3 min of ring constriction, expressed as change in fluorescence intensity. Data shown is mean of nine (Myo2-GFP) or five (Lifeact-GFP) independent experiments; error bars indicate the standard deviation from the mean. (B) Total amount of ring-associated Myo2-GFP at start (open symbols) and after 3 min of constriction (closed symbols). Each color represents a pair in which the larger ring (circles) has constricted to the same circumference as the smaller ring (triangles) at initiation of constriction. The dotted line connects corresponding pairs. The amount of Myo2-GFP is expressed in relative units of fluorescence intensity, as a function of hyphal circumference. (C) Distribution and intensity of Myo2-GFP in a representative pair of rings as described (green dataset) in B. Heat and profile map shows the relative intensity of Myo2-GFP at the start and after 3 min of constriction.

homokaryon (Fig. S3; Pittenger et al., 1954). There was no significant difference in the constriction rates of the heterokaryon Myo2-GFP and the Lifeact-GFP strains, whereas in the homokaryon the constriction rate was reduced by almost 50% (Fig. 8 D). To ensure that the size-dependent increase in myosin concentration during contractile ring assembly was not also a hypomorphic phenotype due to the GFP tag, we measured the relative concentration of Myo2-GFP per unit length and found no difference between the homokaryon and heterokaryon strains (Fig. 8 E). Therefore, the rate of actomyosin ring constriction can be reduced by decreasing either the total amount or the contractile activity of ring-associated myosin II. These findings establish that the size-dependent scalability of actomyosin ring constriction rate in *N. crassa* likely depends upon myosin II.

Discussion

N. crassa is a well-suited model organism for studies of cytokinesis and scalability
In this study, we have determined that hyphal septation in *N. crassa* relies upon a contractile actomyosin ring. Importantly, we identified genes encoding the majority of essential ring components within the *N. crassa* genome, leading us to conclude that this organism shares a basic cytokinetic mechanism with animals

and yeasts. A particularly unique feature of *N. crassa* is that within a single multinucleate coenocytic colony, hyphal circumference can vary over a fourfold range. This intrinsic variability in cell size allows us to look at the size dependence of cellular processes without the need for mutants, drugs, or other perturbations to normal growth and metabolism. This work establishes the use of *N. crassa* as a model for both cytokinesis and for the size-dependent scalability of cellular mechanisms in general.

We have shown that ring constriction in *N. crassa* occurs at a constant rate within a given hyphae and that there is an increase in the rate of ring constriction with increasing initial ring circumference. Previous studies in dividing cells in developing embryos of *C. elegans* have shown that the rate of cytokinesis increases with increasing cell perimeter (Carvalho et al., 2009). That we find a similar cell size–dependent scalability of actomyosin ring constriction rate in *N. crassa* suggests that scalability is likely to be a general property of the contractile mechanism during cytokinesis and not specific to embryonic cell types.

Larger rings assemble with a higher concentration of myosin II, which increases further during constriction
What mechanisms might account for the observed cell size–dependent scalability of ring constriction rates? To investigate the
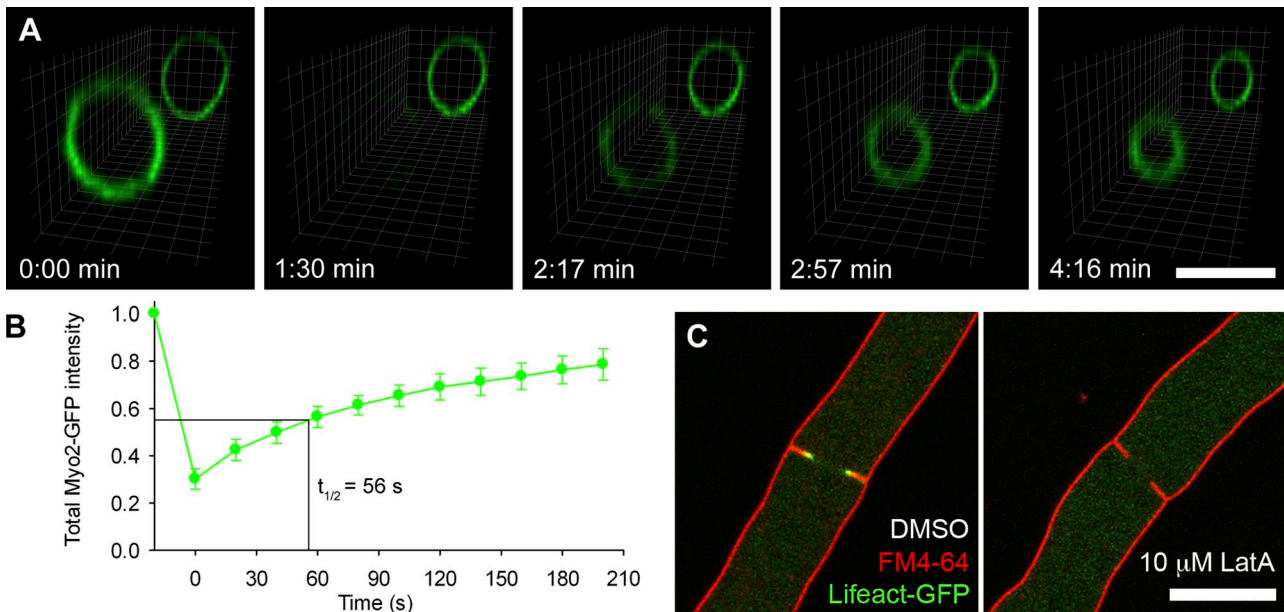
Figure 7. **Turnover of myosin II and F-actin during ring constriction.** (A) Fluorescence recovery after photobleaching (FRAP) of Myo2-GFP in a hypha with two rings in close proximity, rendered into a 3D image. The ring in the foreground was selectively photobleached while the second ring in the background remained unbleached. The time is indicated in minutes. Bar, 10 µm. See also Video 4. (B) Quantitation of FRAP of Myo2-GFP during actomyosin ring constriction. The whole ring was bleached and recovery was monitored as the change in intensity before and after bleaching, corrected for photobleaching resulting from the imaging. Data shown are the mean of 10 independent experiments, expressed in relative units of fluorescence intensity normalized to the corrected prebleach value; error bars represent the standard deviation from the mean. The half time for recovery is indicated on the graph. (C) Observation of Lifeact-GFP (green) and membranes labeled with FM4-64 (red) after inhibition of actin polymerization with DMSO alone (left) or 10 µM latrunculin A (right). Bar, 10 µm.

contributions of the ring components involved in the scalability of ring constriction, we performed the first characterization of myosin II in *N. crassa*. We examined the distribution of myosin II and detected a size-dependent increase in the total amount and concentration of myosin II in the contractile ring upon assembly. The total myosin II levels within the ring remained constant as the ring constricted and thus the concentration increased. The retention of myosin II during ring constriction is a property conserved in many eukaryotes and our findings are in good agreement with this paradigm (Robinson et al., 2002; Wu et al., 2003).

Changes in ring-associated myosin II amount or activity directly affects the rate of ring constriction

One key finding from our study is that an initially larger ring (of circumference *a*) that has constricted to a given size (circumference *b*, where [*a* > *b*]) will contain more myosin than a smaller ring initiating constriction at this same size (circumference *b*). Increased recruitment of myosin II is therefore a pre-constriction property of larger rings that is retained throughout constriction. If this is the property that allows larger rings to constrict at a faster rate, then increasing the recruitment of myosin II to the ring should increase constriction rates further. Though experimental overexpression of myosin II could theoretically address this prediction, a recent study in *S. pombe* (Stark et al., 2010) found that high levels of ectopic expression of myosin II in fact caused a decrease in constriction rates, potentially due to defects in ring assembly. Additionally, studies in *S. pombe* and *D. discoideum* have shown that only 10–27% of the total cytoplasmic pool of myosin proteins accumulate locally at the division

site, suggesting that the cytoplasmic pool of expressed protein is already in excess of the fraction incorporated into the ring (Robinson et al., 2002; Wu and Pollard, 2005). Though to date we have been unable to ectopically increase the amount of ring-associated myosin II, a converse prediction is that decreasing the amount of ring-associated myosin II should decrease constriction rates. Indeed, when we reduced both the total amount and the activity of ring-associated myosin II through blebbistatin treatment or the use of a hypomorphic strain carrying only the Myo2-GFP fusion protein, we observed a resultant decrease in the rate of ring constriction. Based on our findings, we propose that it is not an increased availability of free myosin II but a size-dependent recruitment of myosin II motors to the ring that regulates cell size–dependent scalability of actomyosin ring constriction in *N. crassa*.

How might the accumulation of myosin II in the assembling ring be regulated in a size-dependent way? Recent work examining the force–velocity relationship of myosin II and actin filaments in intact cells determined that reductions in force were primarily due to decreased numbers of myosin motors bound to each filament. This force–velocity relationship was load dependent, such that the number of attached motors was proportional to the filament load (Piazzesi et al., 2007). Given the sensitivity of velocity to an opposing force, increased numbers of myosin motors could speed up ring constriction by increasing contractile force in response to increased load. One size-dependent source of filament load within our system is internal hyphal pressure due to turgor and the force of cytoplasmic mass flow (Lew, 2005). However, because the growing *N. crassa* colony is a coenocytic interconnected system,
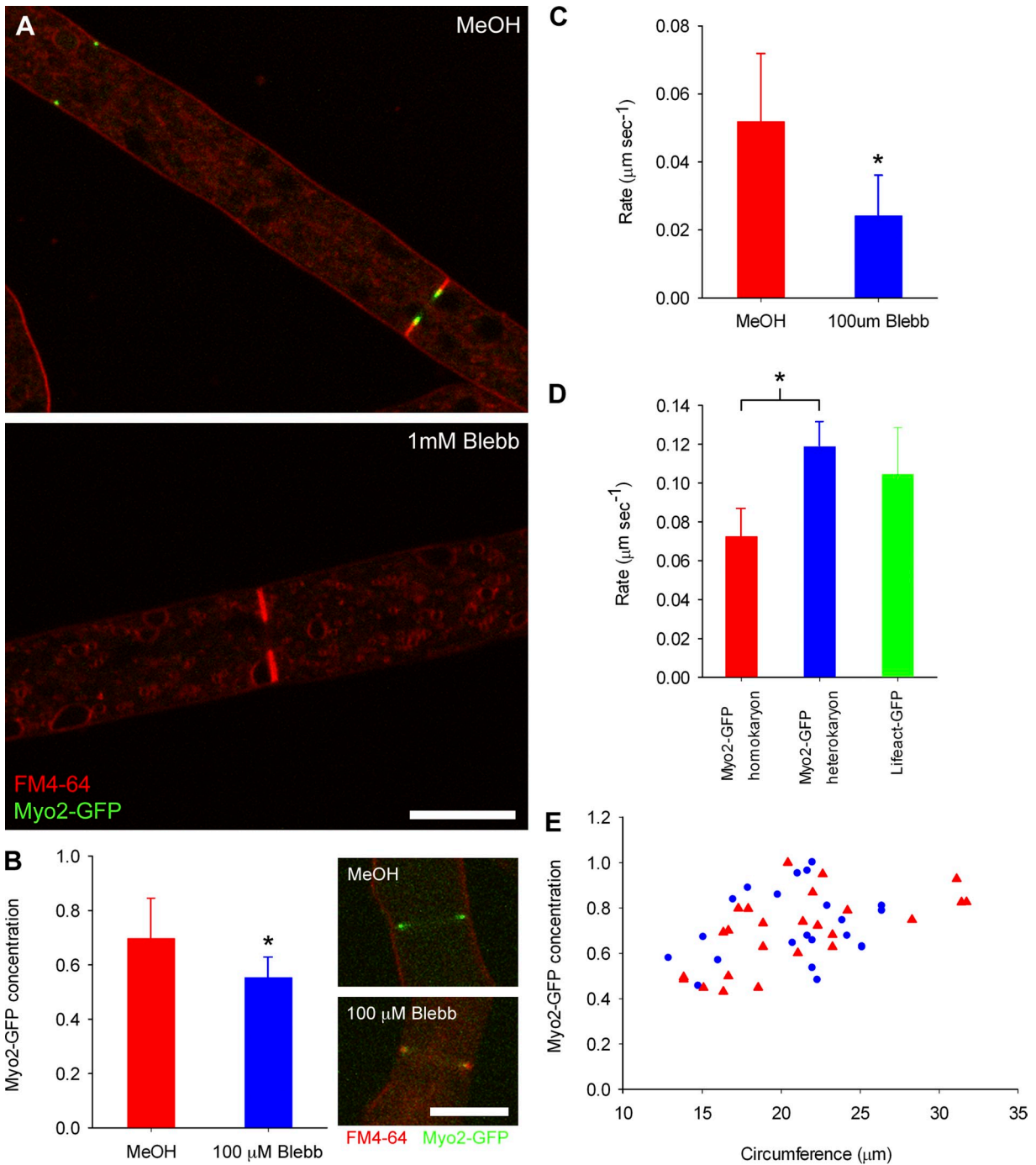
Figure 8. **Inhibition of myosin II after treatment with blebbistatin.** (A) Observation of Myo2-GFP (green) and membranes labeled with FM4-64 (red) after inhibition of myosin II with blebbistatin. MeOH alone as a control (top) and 1 mM blebbistatin (bottom). Bar, 10 μm. (B) Concentration of Myo2-GFP in constricting rings in medium sized cells (mean initial circumference = 25 μm) treated with MeOH alone (red, n = 27, top panel insert) or 100 μM blebbistatin (blue, n = 20, bottom panel insert) expressed in relative units of fluorescence intensity per confocal volume; error bars represent the standard deviation from the mean. Bar, 10 μm. Asterisk indicates statistical significance (unpaired t test; P < 0.0001). (C) Average rate of constriction in medium-sized cells (mean initial circumference = 25 μm) in cells treated with MeOH alone (red, n = 26) or 100 μM blebbistatin (blue, n = 22); error bars represent the standard deviation from the mean. Asterisk indicates statistical significance (unpaired t test, P < 0.0001). See also Video 5. (D) Average rate of constriction in medium-sized cells (mean initial circumference = 25 μm) of the Myo2-GFP homokaryon (red, n = 10), Myo2-GFP heterokaryon (blue, n = 11), and Lifeact-GFP (green, n = 38) strains; error bars represent the standard deviation from the mean. Asterisk indicates statistical significance (unpaired t test, P < 0.0001). (E) Concentration of Myo2-GFP in the Myo2-GFP homokaryon (red triangles, n = 25) and Myo2-GFP heterokaryon (blue circles, n = 22) expressed in relative units of fluorescence intensity per confocal volume, as a function of hyphal circumference.

the turgor pressure should be equivalent across all hyphae and thus size independent. If filament load is equivalent in rings of all sizes, the cortical actin filaments themselves may be reorganized in a size-dependent way as to provide additional myosin-binding sites in larger rings. Studies of both filament distribution and load may shed more light on the mechanism of cytokinesis by uncovering size-dependent differences in actomyosin ring ultrastructure.

The dynamics of actomyosin ring components

The common finding of cell size–dependent scalability of actomyosin ring constriction in *N. crassa* and *C. elegans* suggests that scalability may represent an evolutionarily conserved property of actomyosin ring constriction. However, we have uncovered important mechanistic differences with respect to the dynamics of actin and myosin between these two systems. Though FRAP studies reveal that ring-associated myosin II turns over during constriction as demonstrated here in *N. crassa* and in other systems (Yumura, 2001; Pelham and Chang, 2002), the *C. elegans* study found that myosin in the contractile ring did not undergo rapid exchange with cytoplasmic pools after photobleaching (Carvalho et al., 2009). Unlike myosin II, the total amount of actin in the contractile rings in *N. crassa* decreased throughout constriction. Additionally, inhibition of actin polymerization with latrunculin A revealed that in this system, as in other cell types, the actin filaments in the ring undergo rapid turnover throughout ring constriction (Pelham and Chang, 2002; Guha et al., 2005; Murthy and Wadsworth, 2005). In contrast, treatment of *C. elegans* cells undergoing cleavage furrow constriction with latrunculin A did not impair the progression of cytokinesis (Carvalho et al., 2009). To explore these mechanistic differences, we developed a physical model to explain the size dependence of the contractile mechanism of the actomyosin ring that accounts for the divergent behaviors of the ring components seen in the two systems.

We initially considered an actomyosin ring with myosin motors distributed along its length and actin filaments stably associated throughout constriction. The contractile ring stress is opposed by cytoplasmic viscous stress, so using a radial stress balance the ring constriction rate can be expressed as

$$(-\dot{r}) = \phi R_0 \qquad (1)$$

where $\dot{r}$ is the radial velocity and R_0 is the initial ring radius (Zhang and Robinson 2005). $\phi \equiv 4\pi^2 (f\eta\rho/\mu)$ is the contractile rate constant, where f is the motor force per myosin head, η is the duty ratio, ρ is the concentration of myosin motors per unit length of filament and μ is the viscous dissipation constant. If the concentration of myosin motors ρ is constant, the ring constriction rate scales linearly with the initial ring size and the consequence is full scalability as shown in Fig. 9 A, such that the duration of cytokinesis is independent of initial ring size, a result clearly observed in *C. elegans* embryos (Carvalho et al., 2009).

As shown in Fig. 5 B, the initial myosin concentration in *N. crassa* is not constant, but in fact scales with ring size R_0. Because the myosin concentration varies linearly with ring size, the constriction rate becomes

$$(-\dot{r}) = \phi_0 (\zeta R_0 + 1) R_0 \qquad (2)$$

where ζ is a fitting constant for the size dependent increase in myosin concentration. Larger rings have higher initial myosin concentration ($\zeta > 0$), and therefore cytokinesis is predicted to be completed in a shorter period of time compared with smaller rings, a phenomena we refer to here as *super scalability*, as shown in Fig. 9 B (using $\phi_0 = 0.5$ and $\zeta = 1$). Because the ring constriction rate in *N. crassa* is in fact *partially scalable* and not super scalable, the actual actomyosin ring dynamics cannot be explained by myosin motor activity alone. In vitro studies demonstrate that additional contractile stress can be generated in the absence of motor proteins by the dynamics of actin filaments and their cross-linking proteins alone (Mogilner and Oster, 2003; Footer et al., 2007; Zumdieck et al., 2007). Though actin turnover is distinctly absent in the scalable system, as observed in *C. elegans* (Carvalho et al., 2009), it is possible that actin turnover in *N. crassa* could provide an additional force contribution resulting in partial scalability. Indeed, our Latrunculin A experiment shows that actin is continually turning over in *N. crassa*, as discussed in the preceding sections.

To explore this possibility, we consider an additional myosin-independent contractile force contribution (λ) due to actin turnover:

$$(-\dot{r}) = \phi_0 (\zeta R_0 + 1) R_0 + \lambda. \qquad (3)$$

If the effect of actin turnover were to scale linearly with size, i.e., $\lambda \propto (R_0)^n$ and $n = 1$, then the result would either be full scalability (if $\zeta = 0$) or super scalability (if $\zeta > 0$), as shown in Fig. 9 C. However, if the contribution of actin turnover were to be either independent of initial ring size ($n = 0$) or minimally scalable ($n < 1$), then partial scalability could be possible. Accordingly, we fit the model with our experimental data using parameters $\zeta = 0.3 \pm 0.05$ (slope of Fig. 5 B, top) and $\phi_0 = 0.00085 \pm 0.00015$ s^{-1} (including uncertainty estimates). The best fit of the model to the data are achieved if we input an actin turnover rate of 52 ± 12 nm/s, which is very close to 3 µm/min or 50 nm/s, the typical rate of actin turnover measured in other systems in vivo (Pantaloni et al., 2001). As shown in Fig. 9 D, using these experimentally derived parameters we reach a good agreement between the fitted model and experimental results. Thus, we hypothesize that a size-independent force contribution due to actin turnover, along with the size-dependent variation in myosin motor force, may account for the observed partial scalability in *N. crassa*.

Studies in fission yeast and HeLa cells have revealed that while individual actin filaments progressively disassemble and shorten during ring constriction, the absolute number of filaments within the assembled ring remains constant (Maupin and Pollard, 1986; Kamasaki et al., 2007). Because we find that the amount of myosin II remains constant, the ratio between the absolute number of actin filaments and the number of myosin II motors per filament should also remain constant throughout constriction. We therefore hypothesize that it may be the ratio between the number of motors and the number of actin filaments in a given ring that determines the rate of actomyosin ring constriction during cytokinesis. This would account for why the rate of ring constriction remains constant and does not accelerate, despite the increasing concentration of myosin motors that occurs during constriction.
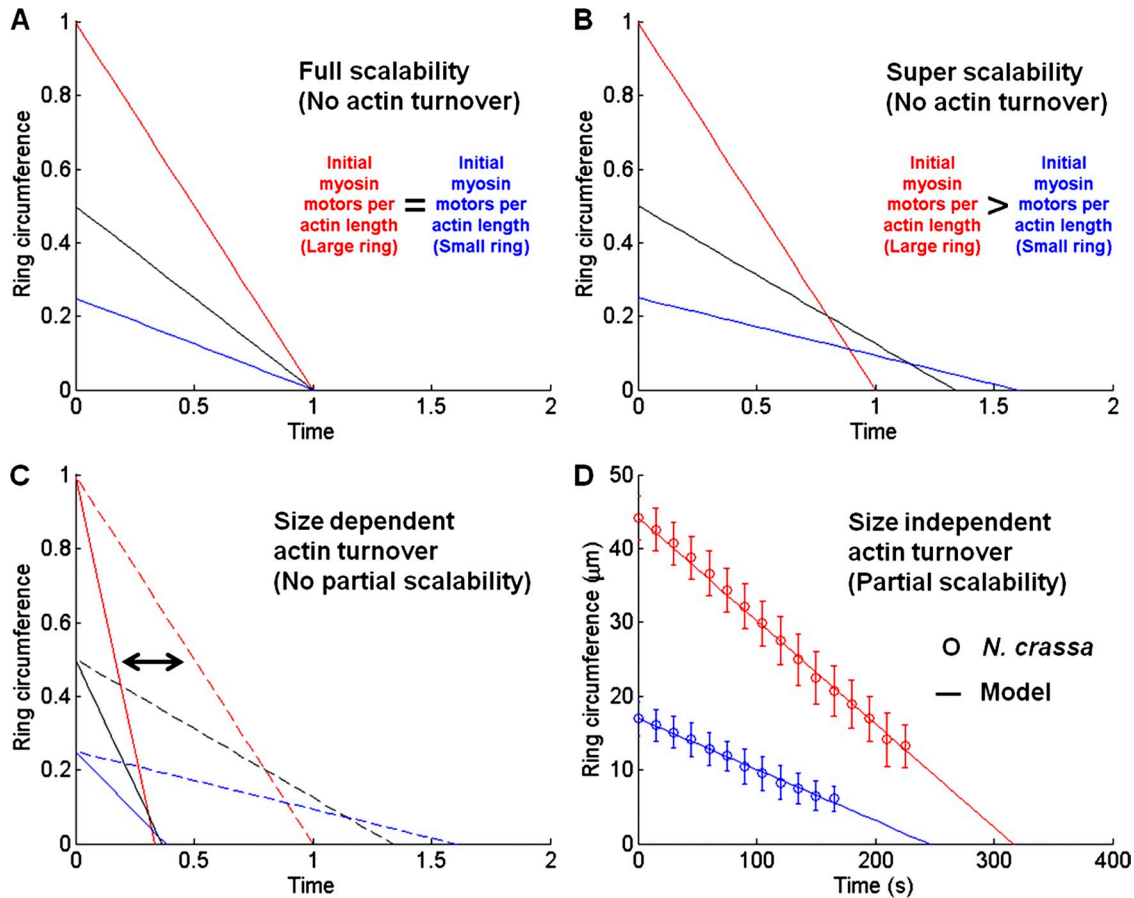
Figure 9. **A physical model for contractile ring dynamics.** (A) Full scalability based on contractile unit hypothesis ($\phi = 1$, $\lambda = 0$). (B) Super scalability due to scalable initial myosin density only ($\phi_0 = 1$, $\zeta = 0.5$, $\lambda = 0$). (C) Size-dependent actin turnover leads to either full scalability (solid lines, $\phi_0 = 1$, $\zeta = 0$) or super scalability (dashed lines, $\phi_0 = 1$, $\zeta > 0$). (D) Size-independent actin turnover leads to partial scalability, as shown in experimental *N. crassa* data (symbols). Model (lines) uses fitted parameters ($\zeta = 0.3 \pm 0.05$, $\phi_0 = 0.00085 \pm 0.00015$ s^{-1} [including uncertainty estimates], and $\lambda = 0.052 \pm 0.012$ µm/s).

What mechanism might account for the size-independent contribution of actin filament turnover? If the actin turnover rate is dependent upon the number of filament ends and the number of filaments scales linearly with ring size, then we would expect to see either full or super scalability, as shown in Fig. 9 C. However, our model predicts that this is not the case. Because the total amount of actin in the newly assembled ring is size dependent (see Fig. 5 A), there are two possibilities that could account for this: either that the individual filaments in larger rings are longer, or that scalable differences in myosin motor density may have a nonlinear effect on the rate of actin turnover. Again, more detailed ultrastructural studies are necessary to directly observe size-dependent differences in actomyosin ring composition.

Summary

In summary, we have demonstrated that the scalability of actomyosin ring constriction is a conserved mechanism among different cell types, and not unique to embryonic cells. Additionally, we find that the assembly of myosin motors into the ring appears to be modulated in a size-dependent way. This may provide additional structural integrity as well as increased velocity to the process of ring constriction. Our findings expand upon

both the understanding of myosin II dynamics and the regulation of actomyosin ring constriction in general. Importantly, our work establishes *N. crassa* as an ideal model system for studying the size dependence of cytokinetic mechanisms in a wild-type and nonembryonic organism.

Materials and methods

Strains and growth conditions
The wild type *N. crassa* strain used was FGSC#9719 (*Δmus52::bar+, mat a*); the Lifeact-GFP construct was inserted into a histidine auxotrophic strain, FGSC#9720 (*his-3-, Δmus52::bar+, mat A*). The *myo2*-deleted heterokaryon was obtained from the *Neurospora* Functional Genomics knockout collection (FGSC#11485). All strains were grown at 30°C on solid Vogel's normal synthetic medium as described previously (Davis and de Serres, 1970).

Construction of Lifeact-GFP expressing strain
The Lifeact-GFP probe was constructed by Klenow extension of the oligonucleotide pair encoding the Lifeact peptide (LA$_F$ and LA$_R$), followed by cloning into the GFP expression plasmid pMF272 (Freitag et al., 2004). Conidia from the *N. crassa* strain FGSC #9720 were transformed with this plasmid by electroporation (Vann, 1995; see Table II for oligonucleotide sequences).

Construction of Myo2-GFP expressing strain
To produce Myo2-GFP, we integrated GFP into the downstream region of the chromosomal locus of *myo2* (NCU00551) into wild-type strain FGSC#9719 using Marker Fusion Tagging (MFT) as described previously

Table II.   **Sequences of oligonucleotides used in this paper**

Name	Sequence
LA_F	5'-GACTACTAGTATGGGCGTCGCCGACCTCATTAAGAAGTTCGAGTCTATTTCCAAGGAGGAGCCCGGGGACT-3'
LA_R	5'-AGTCCCCGGGCTCCT-3'
$Myo2_1$	5'-GGACATTGCTGCTGAGCG-3'
$Myo2_2$	5'-CGGTGAGTTTAGGCTTTTTCATAATAAACCCCTTCGTCAG-3'
$Myo2_3$	5'-TCGGCATGGACGAGCTGTACAAGGCTTTGAGGTGTCTATAG-3'
$Myo2_4$	5'-TGAGCAAGACGTACACAG-3'
$Myo2_5$	5'-CTGACGAAGGGGTTTATTATGAAAAAGCCTAAACTCACCG-3'
$Myo2_6$	5'-CTATAGACACCTCAAAGCCTTGTACAGCTCGTCCATGCCGA-3'

(Ng et al., 2009). The integration fragment was made using the following primers: $Myo2_1$, $Myo2_2$, $Myo2_3$, $Myo2_4$, $Myo2_5$, and $Myo2_6$. Conidia from the *N. crassa* strain FGSC #9719 were transformed with the PCR-generated fragment by electroporation (Vann, 1995; see Table II for oligonucleotide sequences).

Live-cell Imaging
Sample preparation was via the inverted agar block method described previously (Hickey et al., 2005). In brief, the fungal mycelium was grown on agar in a Petri dish, then a block of the agar from the periphery of the colony, measuring 1–4 cm^3 (including the growing hyphal tips) was cut out and gently inverted into a droplet of liquid Vogel's medium (and any required dye or treatment) on a coverslip. Cells were labeled with 1 µM FM4-64 (Invitrogen) and 20 µg/ml calcofluor where noted. For treatment with latrunculin A (Sigma-Aldrich), a 10-mM stock solution was prepared in DMSO and this was diluted into Vogel's medium containing 1 µM FM4-64. The DMSO control was prepared the same way. For treatment with S(-)-blebbistatin (Sigma-Aldrich), a 5-mM stock solution was prepared in MeOH, and this was diluted into Vogel's medium containing 1 µM FM4-64. The MeOH control was prepared the same way. Live-cell imaging was performed at room temperature using a confocal laser scanning microscope (model TCS SP5, Leica; operated with the LAS AF acquisition software) equipped with a Plan Apochromat 63x/1.2 NA water immersion objective lens for imaging and motorized stage used in conjunction with the Mark & Find tool for multi-positional time-lapse acquisition. A multi-line Argon laser (30% output power and 488-nm line set to 40% transmission at the AOTF) was used for the excitation of the GFP (Em. 500–550 nm) and FM4-64 (Em. 568–765 nm) and a 405-nm diode laser (3% transmission at the AOTF) for the calcofluor (Em. 415–478 nm). The standard Leica photomultiplier tubes (PMTs) were used as detectors.

Image processing
Image processing and figure preparations were performed using a combination of Leica LAS AF Lite, Bitplane Imaris (for 3D maximum intensity projection (MIP) volume rendering in Figs. 3 B, 7 A, and Video 3), AutoQuant (for Blind deconvolution for Fig. 3 B), ImageJ (http://rsbweb.nih.gov/ij) and Fiji (http://fiji.sc/wiki/index.php/Fiji) using the LOCI Bioformats (http://www.loci.wisc.edu/bio-formats/about), Stackreg (Thévenaz, et al., 1998; for the kymographs in Figs. 2 E and 3 C), and Adobe Photoshop and SigmaPlot (for figure preparation).

Image analysis methods to determine duration and rates of contractility
The decrease in ring diameter over time was measured for each constriction event. For quantitation of the rate of ring constriction the raw Leica LIF files were opened as stacks in ImageJ using the LOCI Bioformats plugins (http://www.loci.wisc.edu/bio-formats/about). A single smoothing filter was applied to improve the segmentation in the next step. A threshold was then applied to the smoothed stack, and verified to ensure the whole time course of ring constriction was properly segmented. This was then converted to a binary stack for the Object Tracker plugin (http://rsbweb.nih.gov/ij/plugins/tracker.html). Objects smaller than 3 pixels were excluded from the tracking. The plugin outputs the number of objects identified in the binary image, their coordinates, and the distance between them (Fig. S4 A). The data were then taken over to Microsoft Excel and Sigmaplot for further analysis and determination of the duration and rate of constriction. To exclude pre-constriction rings that were still undergoing assembly from the analysis, the first time point of constriction was taken as the first point at which the ring had visibly pulled away from the hyphal cortex. The end point of constriction was considered as the time at which the distance between the points was less than 2 µm (corresponding to a ring circumference

of less than 6.3 µm), as this generally correlated with a significant loss of resolution. Time points during which the ring had drifted from the medial focal plane were excluded from the analysis, and constriction rates were only calculated from rings for which a minimum of five time points were recorded.

Image analysis methods to determine fluorescence intensity and ring-associated protein concentration
For quantitation of the fluorescence intensity and ring-associated protein concentration the raw Leica .lif files were opened in ImageJ using the LOCI Bioformats plugins. To ensure uniformity of illumination across the field of view we performed the field illumination confocal performance test as described by Zucker (2006). There was less than 5% variation over the field of view and no position-dependent correlation of variance was detected. The images were acquired at the medial focal plane, its thickness being determined through the combination of wavelength, objective lens, immersion medium, and confocal pinhole size. The Leica LAS AF software gives a value for confocal slice thickness based on these parameters, which for these experiments was 1.281 µm. Initially the diameter of the ring was measured. Pre-constriction rings that were still undergoing assembly were excluded from the analysis as described above. Two circular regions of interest (9 pixels in diameter) were then drawn over the two intense spots of the ring and their intensities (integrated density) were measured (Fig. S4 B). The data were then taken over to Microsoft Excel where the mean of the two measurements was calculated and used as the protein concentration for that ring. To calculate the total protein in the ring, this average was divided by the confocal volume (a cylindrical volume as the product of the area of the 2D ROI and the confocal slice thickness) and multiplied by the circumference of the ring (Fig. S4 C). Before settling on this methodology, attempts were made to use 3D segmentation to measure the total protein in the ring directly. However, the nature of the sample preparation meant that this was not possible; both the coverslip surface and the agar surface caused artifacts in the imaging such that it was impossible to accurately segment the 3D images.

Fluorescence recovery after photobleaching (FRAP)
FRAP experiments were performed on an inverted confocal laser scanning microscope (model FV1000, Olympus; operated with the Olympus FV-ASW acquisition software) equipped with a Plan Apochromat 60×/1.45 NA oil immersion objective lens at room temperature. For photobleaching, the multi-line Argon laser was set to 30% power on the 488-nm line. An oval ROI encompassing the maximum diameter of the ring was defined and continually bleached (tornado mode) for 8 s, during which time the z-position was adjusted to cover the full extent of the ring. For image acquisition, 8% of the 488-nm laser was used was used for the excitation of GFP (Em. 500–600 nm); one single prebleach z-stack (imaged every 0.8 µm) was acquired, then photobleached, and followed by a time series of the same stack every 20 s for up to 10 min. The standard Olympus PMT was used as a detector. For analysis, using the Fiji software, a sum projection of the stacks was analyzed for the total intensity within the area occupied by the ring. The images were corrected for photobleaching occurring through imaging, using an average of five rings exposed to the same conditions (excluding the FRAP step).

Online supplemental material
Fig. S1 shows mean rates of constriction in primary and secondary hyphae. Fig. S2 shows quantitation of the concentration of ring-associated Lifeact-GFP after treatment with low-dose blebbistatin. Fig. S3 shows quantitation of the concentration of ring-associated Myo2-GFP in homokaryon and heterokaryon strains. Fig. S4 shows image analysis methodology.

Video 1 shows Myo2p-GFP localization during cortical ring formation and constriction. Video 2 shows Lifeact-GFP localization during cortical ring formation and constriction. Video 3 shows membrane formation, cell wall deposition, and actomyosin ring constriction in *N. crassa*. Video 4 shows turnover of myosin II during ring constriction. Video 5 shows that decreased ring-associated myosin II causes a decreased rate of ring constriction. Online supplemental material is available at http://www.jcb .org/cgi/content/full/jcb.201101055/DC1.

References

An, H., J.L. Morrell, J.L. Jennings, A.J. Link, and K.L. Gould. 2004. Requirements of fission yeast septins for complex formation, localization, and function. *Mol. Biol. Cell*. 15:5551–5564. http://dx.doi.org/10.1091/mbc .E04-07-0640

Balasubramanian, M.K., D.M. Helfman, and S.M. Hemmingsen. 1992. A new tropomyosin essential for cytokinesis in the fission yeast *S. pombe*. *Nature*. 360:84–87. http://dx.doi.org/10.1038/360084a0

Balasubramanian, M.K., B.R. Hirani, J.D. Burke, and K.L. Gould. 1994. The *Schizosaccharomyces pombe* cdc3+ gene encodes a profilin essential for cytokinesis. *J. Cell Biol*. 125:1289–1301. http://dx.doi.org/10.1083/ jcb.125.6.1289

Balasubramanian, M.K., D.M. McCollum, L. Chang, K.C. Wong, N.I. Naqvi, X. He, S. Sazer, and K.L. Gould. 1998. Isolation and characterization of new fission yeast cytokinesis mutants. *Genetics*. 149:1265–1275.

Balasubramanian, M.K., E. Bi, and M. Glotzer. 2004. Comparative analysis of cytokinesis in budding yeast, fission yeast and animal cells. *Curr. Biol*. 14:R806–R818. http://dx.doi.org/10.1016/j.cub.2004.09.022

Barr, F.A., and U. Gruneberg. 2007. Cytokinesis: placing and making the final cut. *Cell*. 131:847–860. http://dx.doi.org/10.1016/j.cell.2007.11.011

Barstead, R.J., L. Kleiman, and R.H. Waterston. 1991. Cloning, sequencing, and mapping of an alpha-actinin gene from the nematode *Caenorhabditis elegans*. *Cell Motil. Cytoskeleton*. 20:69–78. http://dx.doi.org/10.1002/ cm.970200108

Berepiki, A., A. Lichius, J.Y. Shoji, J. Tilsner, and N.D. Read. 2010. F-actin dynamics in *Neurospora crassa*. *Eukaryot. Cell*. 9:547–557. http://dx.doi .org/10.1128/EC.00253-09

Bruno, K.S., J.L. Morrell, J.E. Hamer, and C.J. Staiger. 2001. SEPH, a Cdc7p orthologue from *Aspergillus nidulans*, functions upstream of actin ring formation during cytokinesis. *Mol. Microbiol*. 42:3–12. http://dx.doi .org/10.1046/j.1365-2958.2001.02605.x

Carvalho, A., A. Desai, and K. Oegema. 2009. Structural memory in the contractile ring makes the duration of cytokinesis independent of cell size. *Cell*. 137:926–937. http://dx.doi.org/10.1016/j.cell.2009.03.021

Chang, F., D. Drubin, and P. Nurse. 1997. cdc12p, a protein required for cytokinesis in fission yeast, is a component of the cell division ring and interacts with profilin. *J. Cell Biol*. 137:169–182. http://dx.doi.org/10.1083/ jcb.137.1.169

Davis, R.H., and F.J. de Serres. 1970. Genetic and microbiological research techniques for *Neurospora crassa*. *Methods Enzymol*. 17:79–143. http:// dx.doi.org/10.1016/0076-6879(71)17168-6

De Lozanne, A., and J.A. Spudich. 1987. Disruption of the *Dictyostelium* myosin heavy chain gene by homologous recombination. *Science*. 236:1086–1091. http://dx.doi.org/10.1126/science.3576222

Demeter, J., and S. Sazer. 1998. imp2, a new component of the actin ring in the fission yeast *Schizosaccharomyces pombe*. *J. Cell Biol*. 143:415–427. http://dx.doi.org/10.1083/jcb.143.2.415

Eng, K., N.I. Naqvi, K.C. Wong, and M.K. Balasubramanian. 1998. Rng2p, a protein required for cytokinesis in fission yeast, is a component of the actomyosin ring and the spindle pole body. *Curr. Biol*. 8:611–621. http:// dx.doi.org/10.1016/S0960-9822(98)70248-9

Fankhauser, C., A. Reymond, L. Cerutti, S. Utzig, K. Hofmann, and V. Simanis. 1995. The *S. pombe* cdc15 gene is a key element in the reorganization of F-actin at mitosis. *Cell*. 82:435–444. http://dx.doi .org/10.1016/0092-8674(95)90432-8

Field, C.M., M. Coughlin, S. Doberstein, T. Marty, and W. Sullivan. 2005. Characterization of anillin mutants reveals essential roles in septin localization and plasma membrane integrity. *Development*. 132:2849–2860. http://dx.doi.org/10.1242/dev.01843

Footer, M.J., J.W. Kerssemakers, J.A. Theriot, and M. Dogterom. 2007. Direct measurement of force generation by actin filament polymerization using an optical trap. *Proc. Natl. Acad. Sci. USA*. 104:2181–2186. http://dx.doi .org/10.1073/pnas.0607052104

Freitag, M., P.C. Hickey, N.B. Raju, E.U. Selker, and N.D. Read. 2004. GFP as a tool to analyze the organization, dynamics and function of nuclei and microtubules in *Neurospora crassa*. *Fungal Genet. Biol*. 41:897–910. http://dx.doi.org/10.1016/j.fgb.2004.06.008

Galagan, J.E., S.E. Calvo, K.A. Borkovich, E.U. Selker, N.D. Read, D. Jaffe, W. FitzHugh, L.J. Ma, S. Smirnov, S. Purcell, et al. 2003. The genome sequence of the filamentous fungus *Neurospora crassa*. *Nature*. 422:859–868. http://dx.doi.org/10.1038/nature01554

Ge, W., and M.K. Balasubramanian. 2008. Pxl1p, a paxillin-related protein, stabilizes the actomyosin ring during cytokinesis in fission yeast. *Mol. Biol. Cell*. 19:1680–1692. http://dx.doi.org/10.1091/mbc.E07-07-0715

Guha, M., M. Zhou, and Y.L. Wang. 2005. Cortical actin turnover during cytokinesis requires myosin II. *Curr. Biol*. 15:732–736. http://dx.doi.org/ 10.1016/j.cub.2005.03.042

Hara, Y., and A. Kimura. 2009. Cell-size-dependent spindle elongation in the *Caenorhabditis elegans* early embryo. *Curr. Biol*. 19:1549–1554. http:// dx.doi.org/10.1016/j.cub.2009.07.050

Harris, S.D., L. Hamer, K.E. Sharpless, and J.E. Hamer. 1997. The *Aspergillus nidulans* sepA gene encodes an FH1/2 protein involved in cytokinesis and the maintenance of cellular polarity. *EMBO J*. 16:3474–3483. http:// dx.doi.org/10.1093/emboj/16.12.3474

Hickey, P.C., S.R. Swift, M.G. Roca, and N.D. Read. 2005. Live-cell imaging of filamentous fungi using vital fluorescent dyes and confocal microscopy. *In* Methods in Microbiology. T. Savidge and C. Pothoulakis, editors. Elsevier, London, UK. 63–87.

Ishiguro, J., and W. Kobayashi. 1996. An actin point-mutation neighboring the 'hydrophobic plug' causes defects in the maintenance of cell polarity and septum organization in the fission yeast *Schizosaccharomyces pombe*. *FEBS Lett*. 392:237–241. http://dx.doi.org/10.1016/0014-5793 (96)00819-8

Kachur, T., W. Ao, J. Berger, and D. Pilgrim. 2004. Maternal UNC-45 is involved in cytokinesis and colocalizes with non-muscle myosin in the early *Caenorhabditis elegans* embryo. *J. Cell Sci*. 117:5313–5321. http:// dx.doi.org/10.1242/jcs.01389

Kamasaki, T., M. Osumi, and I. Mabuchi. 2007. Three-dimensional arrangement of F-actin in the contractile ring of fission yeast. *J. Cell Biol*. 178:765–771. http://dx.doi.org/10.1083/jcb.200612018

Kitayama, C., A. Sugimoto, and M. Yamamoto. 1997. Type II myosin heavy chain encoded by the myo2 gene composes the contractile ring during cytokinesis in *Schizosaccharomyces pombe*. *J. Cell Biol*. 137:1309–1319. http://dx.doi.org/10.1083/jcb.137.6.1309

Knecht, D.A., and W.F. Loomis. 1988. Developmental consequences of the lack of myosin heavy chain in *Dictyostelium discoideum*. *Dev. Biol*. 128:178–184. http://dx.doi.org/10.1016/0012-1606(88)90280-1

Kovács, M., J. Tóth, C. Hetényi, A. Málnási-Csizmadia, and J.R. Sellers. 2004. Mechanism of blebbistatin inhibition of myosin II. *J. Biol. Chem*. 279:35557–35563. http://dx.doi.org/10.1074/jbc.M405319200

Le Goff, X., F. Motegi, E. Salimova, I. Mabuchi, and V. Simanis. 2000. The *S. pombe* rlc1 gene encodes a putative myosin regulatory light chain that binds the type II myosins myo3p and myo2p. *J. Cell Sci*. 113:4157–4163.

Lew, R.R. 2005. Mass flow and pressure-driven hyphal extension in *Neurospora crassa*. *Microbiology*. 151:2685–2692. http://dx.doi.org/10.1099/mic .0.27947-0

Mabuchi, I., and M. Okuno. 1977. The effect of myosin antibody on the division of starfish blastomeres. *J. Cell Biol*. 74:251–263. http://dx.doi .org/10.1083/jcb.74.1.251

Manstein, D.J., M.A. Titus, A. De Lozanne, and J.A. Spudich. 1989. Gene replacement in *Dictyostelium*: generation of myosin null mutants. *EMBO J*. 8:923–932.

Maupin, P., and T.D. Pollard. 1986. Arrangement of actin filaments and myosin-like filaments in the contractile ring and of actin-like filaments in the mitotic spindle of dividing HeLa cells. *J. Ultrastruct. Mol. Struct. Res*. 94:92–103. http://dx.doi.org/10.1016/0889-1605(86)90055-8

May, K.M., F.Z. Watts, N. Jones, and J.S. Hyams. 1997. Type II myosin involved in cytokinesis in the fission yeast, *Schizosaccharomyces pombe*. *Cell Motil. Cytoskeleton*. 38:385–396.

McCollum, D., M.K. Balasubramanian, L.E. Pelcher, S.M. Hemmingsen, and K.L. Gould. 1995. *Schizosaccharomyces pombe* cdc4+ gene encodes a novel EF-hand protein essential for cytokinesis. *J. Cell Biol.* 130:651–660. http://dx.doi.org/10.1083/jcb.130.3.651

McKim, K.S., C. Matheson, M.A. Marra, M.F. Wakarchuk, and D.L. Baillie. 1994. The *Caenorhabditis elegans* unc-60 gene encodes proteins homologous to a family of actin-binding proteins. *Mol. Gen. Genet.* 242:346–357. http://dx.doi.org/10.1007/BF00280425

Mogilner, A., and G. Oster. 2003. Cell biology. Shrinking gels pull cells. *Science.* 302:1340–1341. http://dx.doi.org/10.1126/science.1092041

Murthy, K., and P. Wadsworth. 2005. Myosin-II-dependent localization and dynamics of F-actin during cytokinesis. *Curr. Biol.* 15:724–731. http://dx.doi.org/10.1016/j.cub.2005.02.055

Nakano, K., and I. Mabuchi. 2006. Actin-depolymerizing protein Adf1 is required for formation and maintenance of the contractile ring during cytokinesis in fission yeast. *Mol. Biol. Cell.* 17:1933–1945. http://dx.doi.org/10.1091/mbc.E05-09-0900

Naqvi, N.I., K.C. Wong, X. Tang, and M.K. Balasubramanian. 2000. Type II myosin regulatory light chain relieves auto-inhibition of myosin-heavy-chain function. *Nat. Cell Biol.* 2:855–858. http://dx.doi.org/10.1038/35041107

Ng, S.K., F. Liu, J. Lai, W. Low, and G. Jedd. 2009. A tether for Woronin body inheritance is associated with evolutionary variation in organelle positioning. *PLoS Genet.* 5:e1000521. http://dx.doi.org/10.1371/journal.pgen.1000521

Nguyen, T.Q., H. Sawa, H. Okano, and J.G. White. 2000. The *C. elegans* septin genes, unc-59 and unc-61, are required for normal postembryonic cytokineses and morphogenesis but have no essential function in embryogenesis. *J. Cell Sci.* 113:3825–3837.

Nurse, P. 1975. Genetic control of cell size at cell division in yeast. *Nature.* 256:547–551. http://dx.doi.org/10.1038/256547a0

Ono, K., and S. Ono. 2004. Tropomyosin and troponin are required for ovarian contraction in the *Caenorhabditis elegans* reproductive system. *Mol. Biol. Cell.* 15:2782–2793. http://dx.doi.org/10.1091/mbc.E04-03-0179

Pantaloni, D., C. Le Clainche, and M.F. Carlier. 2001. Mechanism of actin-based motility. *Science.* 292:1502–1506. http://dx.doi.org/10.1126/science.1059975

Pelham, R.J., and F. Chang. 2002. Actin dynamics in the contractile ring during cytokinesis in fission yeast. *Nature.* 419:82–86. http://dx.doi.org/10.1038/nature00999

Piazzesi, G., M. Reconditi, M. Linari, L. Lucii, P. Bianco, E. Brunello, V. Decostre, A. Stewart, D.B. Gore, T.C. Irving, et al. 2007. Skeletal muscle performance determined by modulation of number of myosin motors rather than motor force or stroke size. *Cell.* 131:784–795. http://dx.doi.org/10.1016/j.cell.2007.09.045

Pinar, M., P.M. Coll, S.A. Rincón, and P. Pérez. 2008. *Schizosaccharomyces pombe* Pxl1 is a paxillin homologue that modulates Rho1 activity and participates in cytokinesis. *Mol. Biol. Cell.* 19:1727–1738. http://dx.doi.org/10.1091/mbc.E07-07-0718

Pittenger, T.H., A.W. Kimball, and K.C. Atwood. 1954. Control of nuclear ratios in *Neurospora* heterokaryons. *Am. J. Bot.* 42:954–958. http://dx.doi.org/10.2307/2485296

Rasmussen, C.G., and N.L. Glass. 2005. A Rho-type GTPase, rho-4, is required for septation in *Neurospora crassa. Eukaryot. Cell.* 4:1913–1925. http://dx.doi.org/10.1128/EC.4.11.1913-1925.2005

Riedl, J., A.H. Crevenna, K. Kessenbrock, J.H. Yu, D. Neukirchen, M. Bista, F. Bradke, D. Jenne, T.A. Holak, Z. Werb, et al. 2008. Lifeact: a versatile marker to visualize F-actin. *Nat. Methods.* 5:605–607. http://dx.doi.org/10.1038/nmeth.1220

Robinson, D.N., G. Cavet, H.M. Warrick, and J.A. Spudich. 2002. Quantitation of the distribution and flux of myosin-II during cytokinesis. *BMC Cell Biol.* 3:4. http://dx.doi.org/10.1186/1471-2121-3-4

Severson, A.F., D.L. Baillie, and B. Bowerman. 2002. A Formin Homology protein and a profilin are required for cytokinesis and Arp2/3-independent assembly of cortical microfilaments in *C. elegans. Curr. Biol.* 12:2066–2075. http://dx.doi.org/10.1016/S0960-9822(02)01355-6

Shelton, C.A., J.C. Carter, G.C. Ellis, and B. Bowerman. 1999. The nonmuscle myosin regulatory light chain gene mlc-4 is required for cytokinesis, anterior-posterior polarity, and body morphology during *Caenorhabditis elegans* embryogenesis. *J. Cell Biol.* 146:439–451. http://dx.doi.org/10.1083/jcb.146.2.439

Skop, A.R., H. Liu, J. Yates III, B.J. Meyer, and R. Heald. 2004. Dissection of the mammalian midbody proteome reveals conserved cytokinesis mechanisms. *Science.* 305:61–66. http://dx.doi.org/10.1126/science.1097931

Stark, B.C., T.E. Sladewski, L.W. Pollard, and M. Lord. 2010. Tropomyosin and myosin-II cellular levels promote actomyosin ring assembly in fission yeast. *Mol. Biol. Cell.* 21:989–1000. http://dx.doi.org/10.1091/mbc.E09-10-0852

Straight, A.F., A. Cheung, J. Limouze, I. Chen, N.J. Westwood, J.R. Sellers, and T.J. Mitchison. 2003. Dissecting temporal and spatial control of cytokinesis with a myosin II Inhibitor. *Science.* 299:1743–1747. http://dx.doi.org/10.1126/science.1081412

Thévenaz, P., U.E. Ruttimann, and M. Unser. 1998. A pyramid approach to subpixel registration based on intensity. *IEEE Trans. Image Process.* 7:27–41. http://dx.doi.org/10.1109/83.650848

Uehara, R., G. Goshima, I. Mabuchi, R.D. Vale, J.A. Spudich, and E.R. Griffis. 2010. Determinants of myosin II cortical localization during cytokinesis. *Curr. Biol.* 20:1080–1085. http://dx.doi.org/10.1016/j.cub.2010.04.058

Vann, D.C. 1995. Electroporation based transformation of freshly harvested conidia of *Neurospora crassa. Fungal Genet. Newsl.* 42A:53.

Velarde, N., K.C. Gunsalus, and F. Piano. 2007. Diverse roles of actin in *C. elegans* early embryogenesis. *BMC Dev. Biol.* 7:142. http://dx.doi.org/10.1186/1471-213X-7-142

Wang, J., H. Hu, S. Wang, J. Shi, S. Chen, H. Wei, X. Xu, and L. Lu. 2009. The important role of actinin-like protein (AcnA) in cytokinesis and apical dominance of hyphal cells in *Aspergillus nidulans. Microbiology.* 155:2714–2725. http://dx.doi.org/10.1099/mic.0.029215-0

Wu, J.Q., and T.D. Pollard. 2005. Counting cytokinesis proteins globally and locally in fission yeast. *Science.* 310:310–314. http://dx.doi.org/10.1126/science.1113230

Wu, J.Q., J. Bähler, and J.R. Pringle. 2001. Roles of a fimbrin and an alpha-actinin-like protein in fission yeast cell polarization and cytokinesis. *Mol. Biol. Cell.* 12:1061–1077.

Wu, J.Q., J.R. Kuhn, D.R. Kovar, and T.D. Pollard. 2003. Spatial and temporal pathway for assembly and constriction of the contractile ring in fission yeast cytokinesis. *Dev. Cell.* 5:723–734. http://dx.doi.org/10.1016/S1534-5807(03)00324-1

Yumura, S. 2001. Myosin II dynamics and cortical flow during contractile ring formation in *Dictyostelium* cells. *J. Cell Biol.* 154:137–146. http://dx.doi.org/10.1083/jcb.200011013

Zhang, W., and D.N. Robinson. 2005. Balance of actively generated contractile and resistive forces controls cytokinesis dynamics. *Proc. Natl. Acad. Sci. USA.* 102:7186–7191. http://dx.doi.org/10.1073/pnas.0502545102

Zucker, R.M. 2006. Quality assessment of confocal microscopy slide based systems: performance. *Cytometry A.* 69:659–676.

Zumdieck, A., K. Kruse, H. Bringmann, A.A. Hyman, and F. Jülicher. 2007. Stress generation and filament turnover during actin ring constriction. *PLoS ONE.* 2:e696. http://dx.doi.org/10.1371/journal.pone.0000696